

Quantum chemical investigation of a new π -conjugated low-bandgap thieno[3,4-b]pyrazine derivative with optoelectronic, photovoltaic and nonlinear optical properties

Mustapha El hadjaoui^a, Mourad Chemek^{b,c}, Mohamed Ouabane^a, Ahmed Azaid^a, Mohamed Riad Fouad^d, Tahar Lakhli^a and Mohammed Bouachrine^{a*}

^aMolecular Chemistry and Natural Substances Laboratory, Faculty of Sciences, Moulay Ismail University of Meknes, Morocco

^bResearch Laboratory: Asymmetric Synthesis and Molecular Engineering of Organic Materials for Organic Electronics (LR18ES19), Faculty of Sciences of Monastir, 5000 Monastir, Tunisia

^cHigher Institute of Applied Sciences and Technology of Sousse, University of Sousse, Sousse, Tunisia

^dDepartment of Pesticide Chemistry and Technology, Faculty of Agriculture, Alexandria University, Aflaton St.El-Shatby, Alexandria, 21545, Egypt

CHRONICLE

Article history:

Received January 1, 2026

Received in revised form

January 12, 2025

Accepted March 9, 2026

Available online

March 9, 2026

Keywords:

Thieno[3,4-b]pyrazine

π -Conjugated donor–acceptor systems

DFT and TD-DFT

Organic photovoltaics

Nonlinear optical properties

ABSTRACT

In this work, we theoretically design a new π -conjugated thieno[3,4-b]pyrazine derivative intended for organic electronics, named 2,3-di([2,2':5',2'':5'',2'''-quaterthiophen]-5-yl)-5,7-bis(5'-(2,5-bis((2-ethylhexyl)oxy)-4-(thiophen-2-yl)-(2,2'-bithiophen)-5-yl)thieno[3,4-b]pyrazine. The geometric, electronic, optical, photovoltaic, and nonlinear optical (NLO) properties of the studied molecule were investigated using calculations based on density functional theory (DFT) and its time-dependent variant (TD-DFT) at the B3LYP/6-31G(d,p) level. The structural modification of the reference molecule results in a small energy gap ($E_g = 1.68$ eV) and a significant enhancement in optical absorption in the visible region, with maxima observed at $\lambda_{\max} = 877$ nm (TD-B3LYP) and $\lambda_{\max} = 668$ nm (CAM-B3LYP). Furthermore, the derived photovoltaic performance indicates a high energy conversion efficiency (PCE $\sim 9.6\%$, $V_{oc} = 0.99$ V) and low excitonic binding energy ($E_b = 0.27$ eV), favorable for efficient exciton separation. The density of states (DOS), frontier molecular orbitals (FMOs), and transition density matrix (TDM) analyses reveal good charge delocalization and strong electronic transfer from the donor to the acceptor. Finally, the high values of the nonlinear optical (NLO) parameters ($\beta_{\text{tot}} = 41.22 \times 10^{-30}$ esu) confirm the strong potential of this molecule for advanced optoelectronic applications.

© 2026 by the authors; licensee Growing Science, Canada.

1. Introduction

Global energy demand is currently a major problem due to over-reliance on conventional energy sources, such as oil, coal, or natural gas, which stimulate secondary deposits underground. This reliance has had severe effects on the human species and deeply harms the state of the environment for future generations. Greenhouse gas emissions are also a consequence^{1, 2}. In such circumstances, the renewable, sustainable, and low-cost energy sources that can phase down emission fouling are a requirement of future energy demand^{3, 5}. Among the options studied, photovoltaic technology is a prominent alternative. Nonetheless, the relatively high costs of c-silicon solar cell production remain as one of the major limitations on its large-scale commercialization^{6, 7}. In response to this limitation, organic solar cells (OSCs) are attracting increasing interest due to their numerous advantages, such as their low toxicity, lightweight, flexibility, ease of implementation, and reduced production cost^{8, 10}. However, the energy conversion efficiency of OSCs is still lower than that of traditional silicon solar cells^{11, 12}; thus, further enhancing their power conversion performance has to be done so as to make them a promising alternative candidate for competing with existing ones. Recent progress, such as the discovery of small-molecule non-fullerene acceptors, has considerably enhanced the performance of OSCs up to a power conversion efficiency (PCE) over 18%, which makes this technology closer to commercial application similar to that for silicon solar cells in the first generation¹³. Organic solar cells mainly come in two architectures: the planar heterojunction, in which the

* Corresponding author

E-mail address m.bouachrine@umi.ac.ma (M. Bouachrine)

© 2026 by the authors; licensee Growing Science, Canada

doi: 10.5267/j.ccl.2026.3.003

donor and acceptor materials are stacked in distinct layers, and the bulk heterojunction (BHJ), which relies on an intimate mixture of the two materials¹⁴. The performance of OSCs essentially depends on the properties of the active layer, which is made of organic materials and represents the heart of the device.

Recently, the combination of electron-rich compounds (donors, D) and electron-poor compounds (acceptors, A) has enabled the design of high-performance π -conjugated semiconductor systems, notably the D–A–D¹⁷ and D– π –A¹⁸ architectures. Among the most studied electron acceptor units is thieno[3,4-*b*]pyrazine, known for its particularly attractive electronic properties. It has found many applications in the areas of organic optoelectronics, such as organic solar cells (OSC)¹⁹, organic light-emitting diodes (OLED)²⁰, and organic field-effect transistors (OFET)²¹, which demand controlled electronic and optical properties. The reference molecule based on thieno[3,4-*b*]pyrazine, recently synthesized by Nathalie Cheminet et al.²², served as the starting point for this study. In this context, we became interested in the incorporation of electron-donating motifs in order to design a new organic material, named 2,3-di([2,2':5',2'':5'',2'''-quaterthiophen]-5-yl)-5,7-bis(5'-(2,5-bis((2-ethylhexyl)oxy)-4-(thiophen-2-yl)phenyl)-[2,2'-bithiophen]-5-yl)thieno[3,4-*b*]pyrazine (TQTP-TPz-TQTP), as illustrated in **Fig. 1**. Using quantum chemistry calculations based on density functional theory (DFT) and its time-dependent version (TD-DFT), we studied its geometric, electronic, optical, photovoltaic, and nonlinear optical properties. The main objective of this work is to improve the optical and photovoltaic performance of the studied molecule for its potential integration into organic photovoltaic devices (OPVs).

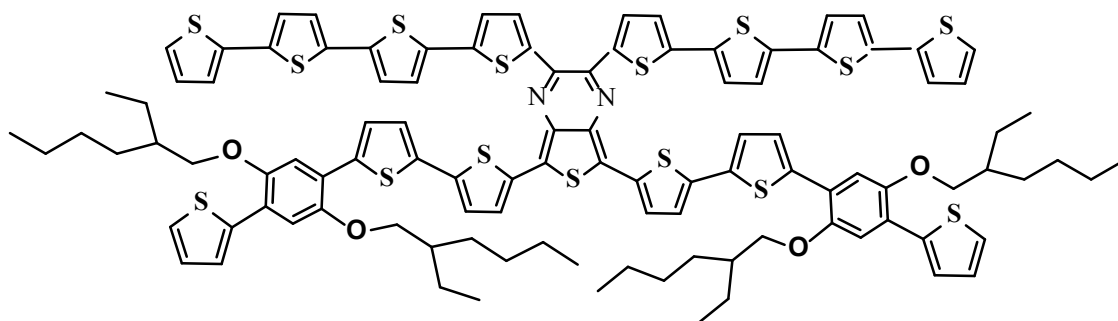


Fig. 1. 2D structure of the studied molecule: 2,3-di([2,2':5',2'':5'',2'''-quaterthiophen]-5-yl)-5,7-bis(5'-(2,5-bis((2-ethylhexyl)oxy)-4-(thiophen-2-yl)phenyl)-[2,2'-bithiophen]-5-yl)thieno[3,4-*b*]pyrazine, denoted as TQTP-TPz-TQTP

2. Synthesis Procedure

Thienopyrazines are heteroaromatic systems incorporating nitrogen and sulfur atoms. These heteroatoms play a crucial role in governing the electronic properties of the molecule. Thienopyrazines act as electron-accepting units in D–A–D (Donor–Acceptor–Donor) architectures, facilitating electron migration from the donor moieties toward the acceptor core, a process that is essential for efficient light absorption and charge transport in organic materials.

To exploit these properties within an extended π -conjugated framework, several synthetic strategies were initially explored. A first approach based on the direct dibromination of thiophene units proved unsuccessful, leading to decomposition of the starting material and preventing the isolation of dibrominated intermediates, even after extensive variation of experimental conditions such as temperature and solvent.

Consequently, the synthetic route was redesigned following a more robust stepwise strategy. The synthesis begins with the dibromination of dinitroterthiophene **1** in DMF using two equivalents of *N*-bromosuccinimide, affording compound **2** in good yield (66%). The use of a highly polar solvent at this stage is essential to overcome the low intrinsic reactivity of the terthiophene derivative. Compound **2** was then subjected to a double Stille cross-coupling reaction with the monostannylated donor **3**, leading to the formation of an extended π -dinitro system **4**. Subsequently, both nitro groups were quantitatively reduced (95%) using iron in acetic acid, yielding the corresponding diamino compound **5** in a highly selective manner. Finally, compound **5** was condensed with the appropriate disubstituted 1,2-diketone **6** to generate the final thienopyrazine derivative **7**, fully integrated into a π -conjugated D–A–D architecture. The overall synthetic pathway is illustrated in **Fig. 2**.²²

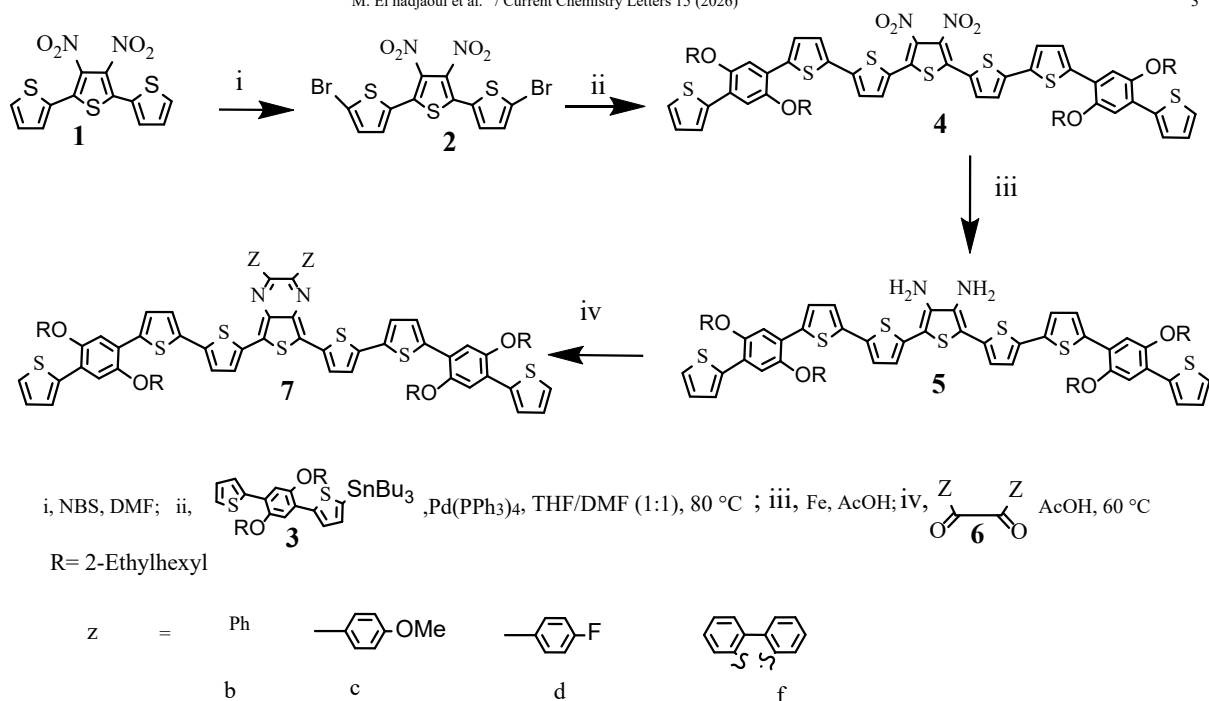
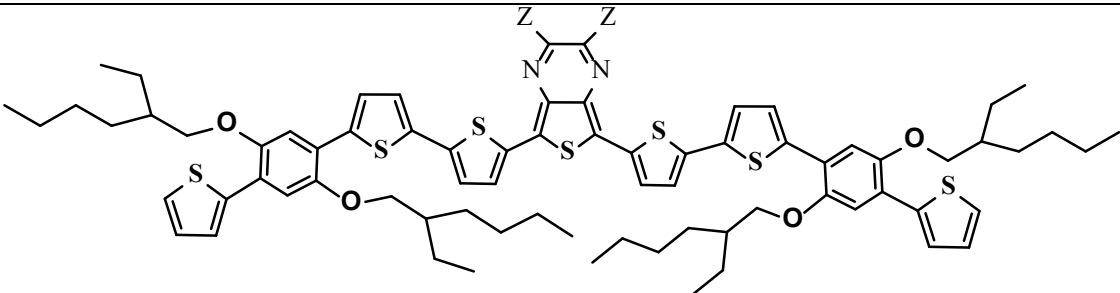


Fig. 2. Synthetic strategy for compound 7 and its derivatives²²

3. Electronic and optical properties of compound 7

The UV–Visible maximum absorption of compounds 7 (b, d, and f) exhibits a significant red shift as a result of the extension of the π -conjugation. Among these derivatives, compound 7f displays an even more extended conjugation, arising from the rigidification of the π -conjugated system into a planar conformation, which is promoted by the presence of a phenanthrene subunit within the molecular backbone. Its experimental UV–Visible spectrum reveals a maximum absorption at 742 nm and a broad absorption spanning the entire visible region (approximately 400–900 nm), indicating a promising potential for organic solar cell applications. In contrast, the absorption properties of compounds 7c and 7d are not significantly affected by the nature of the para-substituent on the phenyl ring (methoxy or fluoro). In the solid state, as drop-cast films prepared from chloroform solutions, compounds 7b–d exhibit a bathochromic shift of 30–50 nm relative to their solution-phase spectra, whereas compound 7f shows only a modest shift (\approx 15 nm). This behavior suggests that compound 7f already adopts a highly planar conformation in solution.

Table 1. Optoelectronic properties of the parent molecule, compound 7²²



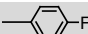
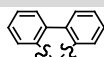
Compound		Energy levels (eV)						Electrochemical band gap	
Z	7	λ_{\max} (nm) (Exp)	λ_{\max} (nm) (DFT)	HOMO (Exp)	HOMO (DFT)	LUMO (Exp)	LUMO (DFT)	E_g (eV) (Exp)	E_g (eV) (DFT)
Ph	b	648	797	-4.49	-4.46	-2.67	-2.61	1.82	1.84
	d	660	783	-4.57	-4.51	-2.64	-2.69	1.93	1.92
	f	742	914	-4.54	-4.37	-2.99	-2.77	1.55	1.60

Table 1 summarizes the frontier molecular orbital (HOMO and LUMO) energy levels, which were determined experimentally by cyclic voltammetry in dichloromethane containing 0.1 M TBAPF₆ and theoretically through DFT calculations. The orbital diagrams indicate that the HOMO is primarily delocalized over the central thiophene units, while the LUMO is predominantly localized on the thienopyrazine subunit, thereby confirming the donor–acceptor character of the system. A good agreement between experimental and calculated values is observed, validating the reliability of the DFT approach for predicting and evaluating the electronic properties of this class of compounds²².

4. Materials and methods

The use of computational chemistry methods is essential in the design and description of the optical-electronic properties for new organic molecules [23, 24]. The 2D structure of the considered molecule was drawn by ChemDraw²⁵ and then visualized in GaussView 6.0. The quantum chemical calculations of all were carried out using the Gaussian 9.0 software package²⁶ based on density functional theory (DFT). The geometric optimization was performed in the gas phase using the hybrid functional B3LYP associated with the 6-31G(d,p) basis set, due to its good balance between accuracy and computational cost, as well as its recognized efficiency in describing the structural and electronic properties of π -conjugated organic systems^{27, 30}. The optical properties (absorption and emission), the density of electronic states (DOS), the transition density matrix (TDM), and the nonlinear optical (NLO) properties were calculated using the TD-B3LYP and CAM-B3LYP methods³¹. The absorption, emission, DOS curves, and Scharber diagram were plotted using Origin 7.0 software [32], while the visualization of TDM maps and NLO properties was done using the multiwfn program³³.

5. Results and discussion

5.1. Geometric properties

Electronic charge delocalization is promoted by both the extension of the π -conjugated backbone and the increased planarity of the molecular framework^{17,34}. In order to verify this deduction, it is necessary to calculate the bond lengths (d_i ($i = 1 - 8$)) and dihedral angles (θ_i ($i = 1 - 8$)) of the studied molecule. To do this, the geometric optimization of the molecule was carried out in the gas phase using the hybrid functional B3LYP with the 6-31G(d,p) basis set, as shown in **Fig. 3**, **Table 2**, and **Table 3**. From these results, we observe that the dihedral angles range between 147.32° and 176.89°, which indicates that the molecule adopts an overall quasi-planar structure, with slight conformational distortions. This quasi-planarity is particularly favorable for an efficient π conjugation between the different constituent units of the molecule. Regarding the bond lengths, they are very homogeneous, ranging between 1.43 Å and 1.46 Å, which indicates an intermediate character between single (C-C) and double (C=C) bonds. These values confirm that there is a good conjugation along the molecule and an efficient delocalization of π bonds, which would in turn provide structural stability and optoelectronic properties to the molecule.

Table 2. Dihedral angles θ_i of the studied molecule

Molecule	θ_1	θ_2	θ_3	θ_4	θ_5	θ_6	θ_7	θ_8
TQTP-TPz-TQTP	147.32	-174.31	165.93	-163.72	176.89	165.63	166.09	-152.32

Table 3. Bond lengths d_i of the studied molecule

Molecule	d_1	d_2	d_3	d_4	d_5	d_6	d_7	d_8
TQTP-TPz-TQTP	1.46	1.44	1.44	1.44	1.43	1.44	1.46	1.46

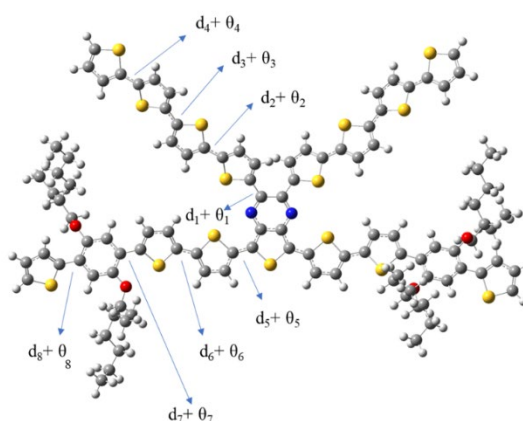


Fig. 3. Optimized structure of the TQTP-TPz-TQTP molecule

5.2 The frontier molecular orbitals (FMOs) and the density of electronic states (DOS)

The band gap is one of the most important parameters to describe optoelectronic properties because it represents the energy difference between the lowest unoccupied molecular orbital (LUMO) and highest occupied molecular orbital (HOMO), according to Eq. (1)^{35, 36}. These energy levels were calculated using quantum chemistry and density functional theory (DFT) with the hybrid functional B3LYP/6-31G(d,p). The final data obtained are $E_{LUMO} = -2.71$ eV, $E_{HOMO} = -4.39$ eV, and $E_g = 1.68$ eV (see **Table 4**). Note that these electronic features are indicative of the effective π conjugation and suitable alignment of frontier orbitals, which provides insightful physical pictures for the studied molecule as an ideal candidate for OSCs. Indeed, such an energy gap promotes an efficient separation of charges and induces a bathochromic shift of optical absorption toward longer wavelengths, thus leading to a higher value of λ_{max} . Frontier molecular orbitals (HOMO/LUMO) constitute essential parameters for understanding the optical and electronic properties of π -conjugated molecular systems. They allow for the analysis of the distribution, separation, and delocalization of electronic charges along the molecular chain. According to the literature, the electronic transition from the ground state (HOMO) to the excited state (LUMO) must occur in organic polymeric materials intended for optoelectronic applications. The spatial distribution of these orbitals and the associated charge distribution are illustrated in **Fig. 4**. In this work, the electron density associated with the HOMO orbital is mainly distributed on the donor units of the molecule, while the electron density of the LUMO orbital is localized on the pyrazine core (acceptor). This separation of electron densities highlights a better charge separation as well as an efficient intramolecular charge transfer (ICT) between the donor and acceptor units. In order to confirm the previous results, a theoretical study based on DFT, using the hybrid functional B3LYP/6-31G(d,p), was conducted to generate the curves of the electronic density of states (DOS), as illustrated in **Fig. 5**. The calculations demonstrate a considerable charge separation, where HOMO orbitals are well localized on the donor moieties, while the LUMO orbitals are centered on the acceptor units, indicating efficient intramolecular delocalization of charges between donor/acceptor segments. The combined analysis of frontier molecular orbitals (FMOs) and density of electronic states (DOS) reveals a pronounced donor–acceptor–type separation, validating the strong potential of this system for high-performance optoelectronic applications in organic devices.

$$E_g = E_{LUMO} - E_{HOMO} \quad (1)$$

Table 4. E_{HOMO} , E_{LUMO} , and E_g values (eV) of the studied molecule

Molecule	E_{HOMO}	E_{LUMO}	E_g
TQTP-TPz-TQTP	-4.39	-2.71	1.68

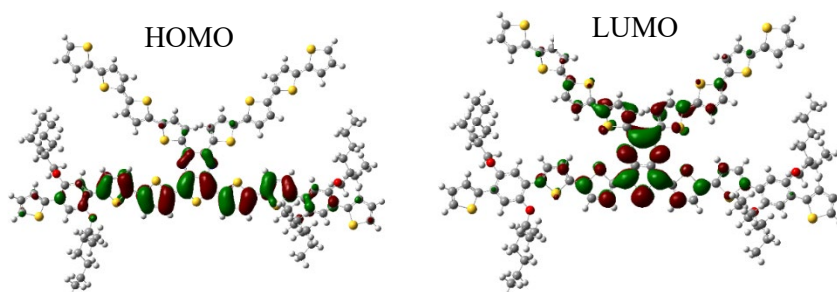


Fig. 4. Electronic distribution of the HOMO and LUMO orbitals

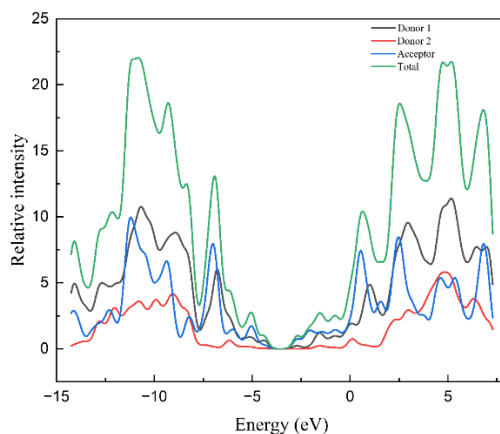


Fig. 5. Electronic density of states (DOS)

5.3 Reactivity indices

Some global chemical descriptors, calculated according to Koopman's theorem³⁷, were determined in order to assess the chemical reactivity of the studied molecule. These include the energies of the frontier orbitals, the HOMO (E_{HOMO}) and LUMO (E_{LUMO}), as well as the energy gap, E_g , which are important descriptors of the electronic properties of molecular systems. These values also allow for the calculation of other key chemical parameters, including the chemical potential (μ), electronegativity (χ), chemical hardness (η), chemical softness (S), and electrophilicity index (ω)^{38,39}.

In addition, electron affinity (EA) and ionization potential (IP) were also considered, as they are used for the study of charge transfer mechanisms and electronic stability⁴⁰. The calculation of all these parameters was carried out using equations (2–8)⁴¹, and the obtained values provide a deep understanding of the reactivity, electronic stability, and overall chemical properties of the studied molecule⁴². **Table 5** shows that the value of IP = 4.39 eV suggests that the studied molecule can easily lose electrons, thus indicating an appreciable donor character. In parallel, the high value of the electron affinity (EA = 2.71 eV) indicates an effective ability of the molecule to accept electrons, which highlights its acceptor character. According to the above results, as a D–A–D-type molecule suitable for effective charge separation and transport, the studied molecule seems to be promising for application of OSCs.

The calculated values of the chemical descriptors are $\mu = -3.55$ eV, $\eta = 0.84$ eV, $\chi = 3.55$ eV, $S = 0.59$ eV⁻¹, and $\omega = 7.51$ eV. All these global reactivity parameters reveal that TQTP-TPz-TQTP exhibits an optimal balance between electronic stability and chemical reactivity, characterized by high chemical flexibility and a significant electrophilicity index. These characteristics are particularly favorable for charge transfer processes, electronic polarization, and intermolecular interactions, thus confirming the high potential of the molecule as an active material for advanced optoelectronic applications, notably organic solar cells and devices with efficient charge transport⁴³.

$$IP = -E_{HOMO} \quad (2)$$

$$EA = -E_{LUMO} \quad (3)$$

$$\mu = (E_{HOMO} + E_{LUMO}) / 2 \quad (4)$$

$$\eta = (E_{LUMO} - E_{HOMO}) / 2 \quad (5)$$

$$\chi = -\mu = -(E_{HOMO} + E_{LUMO}) / 2 \quad (6)$$

$$S = 1/(2\eta) = 1/(E_{LUMO} - E_{HOMO}) \quad (7)$$

$$\omega = \frac{\mu^2}{2\eta} \quad (8)$$

Table 5. Chemical reactivity indices of the studied molecule

molecule	IP (eV)	EA (eV)	(eV) μ	η (eV)	χ (eV)	S (eV ⁻¹)	(eV) ω
TQTP-TPz-TQTP	4.39	2.71	-3.55	0.84	3.55	0.59	7.51

5.4. Molecular electrostatic potential (MEP)

The molecular reactivity is further analyzed by molecular electrostatic potential surface (MEP) maps based on the electron density. The 3-D cartoon map provides a three-dimensional representation of the spatial distribution of electrical charges over the entire molecule, arising from interactions between atoms^{44,45}. The MEP has been widely applied to identify nucleophilic and electrophilic sites, as well as to predict hydrogen bonding locations^{46,47}.

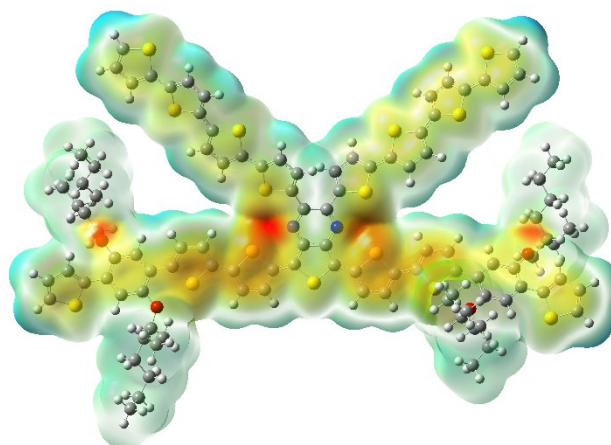


Fig. 6. Three-dimensional map of the molecular electrostatic potential (MEP)

The MEP map (Fig. 6) is characterized by different colors corresponding to the electrostatic potential: red regions are electron-rich and favorable for nucleophilic attacks, blue areas are electron-poor, suitable for electrophilic interactions, and green regions are neutral. The magnitude of the electrostatic potential is ordered as follows: red>orange>yellow>green>blue⁴⁸. On the MEP map of the studied molecule, the red (negative potential) regions are located on the oxygen atoms, while yellow areas are observed around sulfur atoms. These regions contain an abundance of electrons, as reflected by their nucleophilic character. Positive potential (blue) is observed around the hydrogen atoms, which can interact with nucleophilic species; this charge distribution appears to be favorable for the optoelectronic properties of the system.

5.5. Optical properties

The theoretical optical properties of the molecule under investigation were also analyzed through quantum chemistry computations based on time-dependent density functional theory (TD-DFT) method using B3LYP/6-31G(d,p) and CAM-B3LYP hybrid functionals. These methods provide detailed dynamical information on electronic excitations. The plot of the absorption curves obtained by these two approaches is shown in Fig. 7.

The main photophysical parameters, namely the maximum absorption wavelength (λ_{\max}), the oscillator strength (f), the vertical excitation energies (E_{ex}), the nature of the major transitions (MO), the percentage contribution, as well as the light-harvesting efficiency (LHE), are summarized in Table 6. Fig. 7 presents two absorption spectra: one obtained using the TD-B3LYP functional and the other using the CAM-B3LYP functional. In the case of the B3LYP functional, the molecule absorbs in the visible region between $\lambda_{\max} = 651$ nm and $\lambda_{\max} = 877$ nm, showing a strong redshift, with excitation energies ranging between $E_{\text{ex}} = 1.90$ eV to $E_{\text{ex}} = 1.41$ eV. On the other hand, the CAM-B3LYP functional shows that the studied molecule absorbs in the visible range and presents three main absorption bands at $\lambda_{\max} = 439$ nm, $\lambda_{\max} = 488$ nm, and $\lambda_{\max} = 668$ nm, corresponding respectively to excitation energies of $E_{\text{ex}} = 2.82$ eV, $E_{\text{ex}} = 2.53$ eV, and $E_{\text{ex}} = 1.85$ eV. The value of the oscillator strength (f) provides important information about the efficiency of light capture (LHE). In order to calculate the light-harvesting efficiency, Eq. (9) is used⁴⁹.

$$\text{LHE} = 1 - 10^{-f} \quad (9)$$

High LHE can lead to enhanced photocurrent generation and behavior that is advantageous to the overall performance of PV devices⁵⁰. For the CAM-B3LYP functional, the highest-intensity transition occurs at $f = 0.90$ with an LHE = 0.87. This band can be mainly ascribed to the HOMO \rightarrow LUMO transition (91%), which suggests that this excitation has a strong $\pi \rightarrow \pi^*$ character with pronounced ICT. On the other hand, the TD-B3LYP functional shows a HOMO \rightarrow LUMO transition (99%) with a more moderate oscillator strength ($f = 0.57$) and a light-harvesting efficiency (LHE) = 0.73. The strong bathochromic shift observed with the B3LYP functional is attributed to the overestimation of the intramolecular charge-transfer character, while the CAM-B3LYP functional, thanks to its long-range correction, provides a more realistic description of electronic excitations involving $\pi \rightarrow \pi^*$ and ICT transitions. In addition, the investigated molecule possesses excellent optoelectronic performance, which suggests that it is a potential candidate for organic solar cells.

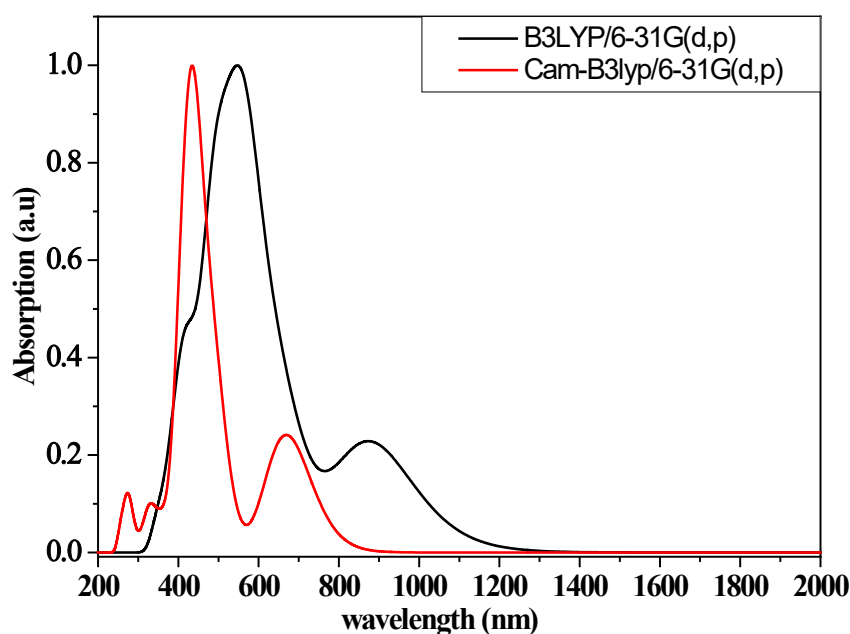
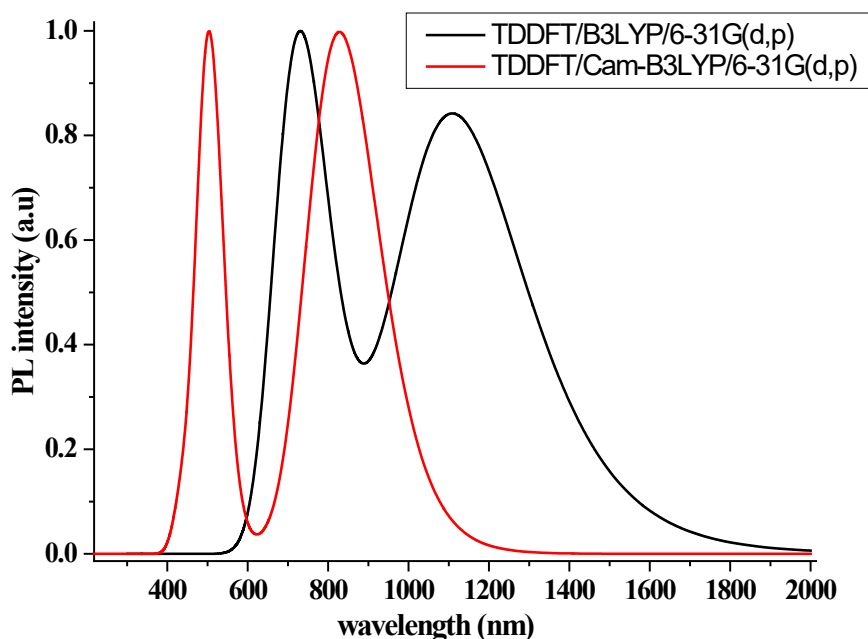


Fig. 7. UV-Visible spectrum of the studied molecule (TD-B3LYP and CAM-B3LYP)

Table 6. Maximum absorption wavelengths (λ_{\max}), excitation energies (E_{ex}), oscillator strengths (f), and light-harvesting efficiency (LHE) of the studied molecule obtained using TD-B3LYP and CAM-B3LYP

Méthode	λ_{\max} (nm)	E_{ex} (eV)	f	LHE	MO/caracter
CAM-B3LYP	668	1.85	0.90	0.87	HOMO→LUMO (91%)
	488	2.53	1.26		H-1→LUMO (58%)
	439	2.82	2.73		H-3→LUMO (26%)
TD-B3LYP	877	1.41	0.57	0.73	HOMO→LUMO (99%)
	668	1.85	0.22		H-1→LUMO (84%)
	651	1.90	0.50		HOMO→L+1 (83%)

The emission properties of the studied molecule were extracted by re-optimization of the optimized chemical structure in the first excited state using the TD-DFT/B3LYP/6-31G(d,p) and TD-DFT/CAM-B3LYP/6-31G(d,p) level of theory. The simulated photoluminescence (PL) spectra were first generated using Gaussview then using GaussSum software, and are presented in **Fig. 8**. Emission in the red–near-infrared region is obtained, with two maximum emission peaks at around 733 and 1110 nm (TD-DFT/B3LYP/6-31G(d,p), and at around 500 and 830 nm (TD-DFT/CAM-B3LYP/6-31G(d,p).

**Fig. 8.** Simulated PL spectra of the studied molecule using the TD-DFT/B3LYP/6-31G(d,p) and the TD-DFT/CAM-B3LYP/6-31G(d,p) level of theory

5.6. Photovoltaic properties

The energies of the frontier molecular orbitals, HOMO and LUMO, are key parameters for evaluating the photovoltaic performance of organic solar cells (OPVs), particularly through the open-circuit voltage (V_{oc}) and the energy shift of the LUMO level (α). The V_{oc} corresponds to the maximum voltage delivered in the absence of current⁵¹ and can be theoretically calculated as the difference between the energy of the HOMO orbital of the donor and that of the LUMO orbital of the acceptor, according to Eq. (10)^{52, 53}.

$$V_{\text{oc}} = \frac{1}{e} (|E_{\text{HOMO}}(\text{Donor})| - |E_{\text{LUMO}}(\text{Acceptor})|) - 0.3 \quad (10)$$

where e is the elementary charge and 0.3 eV is an empirical factor related to the binding energy of excitons⁵⁴.

The LUMO offset (α), defined as the difference between the LUMO level of the donor and the acceptor, plays a crucial role in the efficient dissociation of excitons and the generation of free charges in organic solar cells^{55, 57}, according to Eq. (11).

$$\alpha = E_{\text{LUMO}}(\text{Donor}) - E_{\text{LUMO}}(\text{Acceptor}) \quad (11)$$

In this work, the parameters V_{oc} and α were calculated for the studied molecule in combination with different fullerene-based acceptors (PCBM, BisPCBM, PC₇₀BM, and ICBA), with the results illustrated in **Table 7**. The values of V_{oc} vary

depending on the acceptor used and can be ranked in ascending order as follows: V_{oc} (PC₇₀BM) = 0.39 V < V_{oc} (PCBM) = 0.49 V < V_{oc} (BisPCBM) = 0.89 V < V_{oc} (ICBA) = 0.99 V. Regarding the LUMO energy shift (α), all donor/acceptor combinations show values above the minimum threshold of 0.3 eV. These values increase in the following order: α (ICBA) = 0.38 eV < α (BisPCBM) = 0.48 eV < α (PCBM) = 0.88 eV < α (PC₇₀BM) = 0.98 eV. These results show that the TQTP-TPz-TQTP molecule exhibits high V_{oc} values as well as an adequate α shift, confirming efficient charge dissociation and potentially optimal photovoltaic performance. Thus, this molecule appears to be a potential candidate for organic solar cell applications.

Table 7. Calculated values of E_{HOMO} , E_{LUMO} , V_{oc} , and α for the studied molecules with different acceptors (ICBA, PC₇₀BM, BisPCBM, and PCBM)

Molecule/ accepteurs	E_{HOMO}	E_{LUMO}	PCBM		BisPCBM		PC ₇₀ BM		ICBA	
			V_{oc} (V)	α	V_{oc} (V)	α	V_{oc} (V)	α	V_{oc} (V)	α
TQTP-TPz-TQTP	-4.39	-2.71	0.49	0.88	0.89	0.48	0.39	0.98	0.99	0.38
PCBM	-5.66	-3.60	-	-	-	-	-	-	-	-
BisPCBM	-5.65	-3.20	-	-	-	-	-	-	-	-
PC ₇₀ BM	-5.55	-3.70	-	-	-	-	-	-	-	-
ICBA	-5.64	-3.10	-	-	-	-	-	-	-	-

5.7 Scharber Model

The Scharber model is widely used as a computational approach for predicting the energy conversion efficiency of organic photovoltaic materials^{53, 61, 62}. According to this model, the estimation of the power conversion efficiency (PCE) mainly depends on the energy gap (E_g) of the studied molecule as well as the energy shift of the LUMO level (α)⁶³, the corresponding results are presented in Fig. 8 and Table 8.

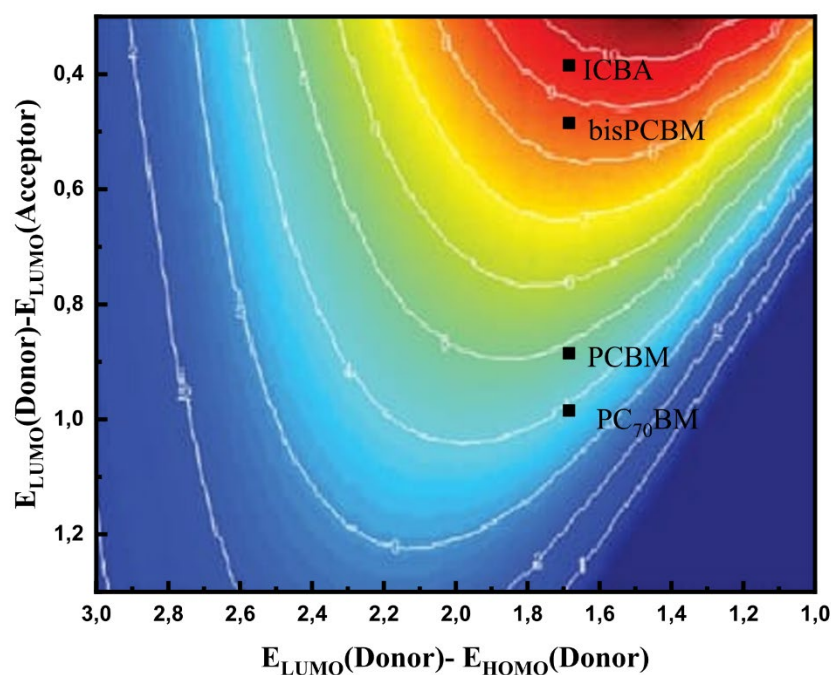


Fig. 8. Contour plots showing the power conversion efficiency of the studied compound

We notice that the PCE dramatically changes depending on the acceptor employed. The best photovoltaic performances are obtained with the ICBA and BisPCBM acceptors, both showing low α values, yielding PCEs of 9.6% and 8.7%, respectively. These results indicate good energy level alignment between the donor and acceptor, leading to a high open-circuit voltage (V_{oc}). In contrast, the PCBM and PC₇₀BM acceptors show higher α values and lower PCEs (~ 5% and ~ 4%). This reduction in efficiency is due to the occurrence of higher energy losses during exciton splitting. Accordingly, the ICBA and BisPCBM acceptors are expected to lead to high-efficiency organic solar cells (OSCs).

Table 8. Power conversion efficiencies (PCE, %) estimated using the Scharber model

Acceptor	TQTP-TPz-TQTP ($E_g = 1.68$ eV)	
	α	PCE (%)
PCBM	0.88	~ 5%
BisPCBM	0.48	~ 8.7%
PC ₇₀ BM	0.98	~ 4%
ICBA	0.38	~ 9.6%

5.8 Nonlinear optical properties (NLO)

The nonlinear optical (NLO) responses of organic materials originate from their response to high-field electromagnetic waves⁶⁴. Understanding these NLO parameters is fundamentally important because of their broad applicability in modern technologies such as optical communication, data storage, telecommunications, and information processing^{65, 66}. Investigation of NLO parameters is crucial for enhancing the optoelectronic properties of organic materials and, in particular, for activating intramolecular charge delocalization. π -Conjugated systems have been appealing for such applications due to their synthetic accessibility and typically exhibit high hyperpolarizability⁶⁷.

The polarizability (α) and total hyperpolarizability (β_{tot}) were evaluated within the framework of quantum-chemistry calculations using TD-DFT approach with the hybrid functional B3LYP/6-31G(d,p). The polarizability α and the total hyperpolarizability (β_{tot}) are obtained using Eqs. (12-14), and the results are listed in **Table 9**. The investigated molecule has an average polarizability $\alpha = 355.19 \times 10^{-24}$ esu, which indicates a high linear response to electric fields. This property is common for long π -conjugated systems and is advantageous for optoelectronic applications. On the other hand, the high value of the total hyperpolarizability $\beta_{\text{tot}} = 41.22 \times 10^{-30}$ esu, compared to that of urea⁶⁸ ($\beta_{\text{tot}} = 0.3728 \times 10^{-30}$ esu), confirms the strong nonlinear character of the TQTP-TPz-TQTP molecule. This NLO performance can be attributed to the extended π conjugation, the presence of donor-acceptor units rich in heteroatoms, and an electronic distribution that favors intramolecular charge delocalization. These results indicate that TQTP-TPz-TQTP is a high-performance NLO material and may have potential applications in modern optoelectronics.

$$\alpha = \frac{1}{3} (\alpha_{xx} + \alpha_{yy} + \alpha_{zz}) \quad (12)$$

$$\beta_{\text{tot}} = \sqrt{\beta_x^2 + \beta_y^2 + \beta_z^2} \quad (13)$$

where xx , yy , and zz represent the tensor components of polarizability, and β_i ($i = x, y, z$) correspond to the hyperpolarizability components given by:

$$\beta_i = \left(\frac{1}{3}\right) \sum_{i=x,y,z} (\beta_{ijj} + \beta_{jij} + \beta_{jji}) \quad (14)$$

Table 9. Polarizability (α) and first hyperpolarizability (β_{tot}) of the studied molecule

Studied molecule	TQTP-TPz-TQTP
α_{xx}	4089.64
α_{xy}	-27.52
α_{yy}	2282.73
α_{xz}	58.00
α_{yz}	72.51
α_{zz}	817.42
α (a.u.)	2396.59
α (10^{-24} esu)	355.19
β_{xxx}	194.30
β_{xxy}	-10230.30
β_{xyy}	724.51
β_{yyy}	14458.60
β_{xxz}	-227.75
β_{xyz}	-2604.04
β_{yyz}	1591.95
β_{xzz}	-425.33
β_{yzz}	258.20
β_{zzz}	189.30
β_{tot} (a.u.)	4773.43
β_{tot} (10^{-30} esu)	41.22

5.9 Transition density matrix (TDM)

The Transition density matrix (TDM) is a model parameter for the charge-transfer mechanism in molecular systems⁶⁹. It is commonly represented graphically by heat maps showing the distribution and extent carrier localization in electronic transitions⁷⁰. This analysis therefore allows identification of donor-acceptor interactions, while the contribution of hydrogen atoms can be neglected as they are less involved in these transitions. The TDM for the studied molecule was calculated using TD-DFT at the B3LYP/6-31G(d,p) level with the Multiwfn program (**Fig. 9**). The TDM map of the studied molecule shows intense signals along the diagonal, which provides evidence that the electronic transition is basically localized. This transition is of the $\pi \rightarrow \pi^*$ type, with spatially well-overlapping frontier orbitals. This situation is beneficial for the efficient

light absorption (optical absorption enhancement); furthermore, the electronic localization can help establish strong interfacial charge transfer to the acceptor, contributing to improved OPV performance.

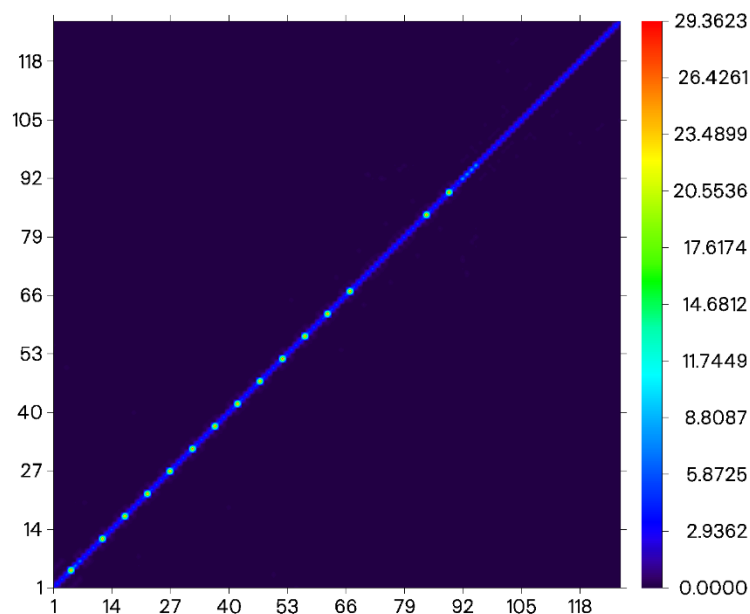


Fig. 9. Transition density matrix (TDM) maps of the four studied molecule calculated at the B3LYP/6-31G(d,p) level and computed in the Multiwfn program arbitrary units (A.U.)

5.10 Exciton Binding Energy (E_b)

The binding energy E_b is a fundamental electronic parameter. It enables the study of exciton dissociation and Coulomb correlations, two effects that fundamentally control the efficiency of organic photovoltaic devices⁷¹. A small binding energy E_b separates photoinduced charges and generates as much current as possible. For this reason, a decrease in E_b is generally associated with an increase in PCE, and this parameter represents an important handle for solar cell optimization⁷². The binding energy of excitons is calculated according to Eq. (15)⁷³. **Table 10** presents the results obtained. The studied molecule has a small E_b value of 0.27 eV, implying that little energy is necessary for exciton separation. This value (less than 0.3 eV) also confirms the ease of producing free charges. These results imply high PCE for the studied molecule, making it attractive for applications in organic photovoltaic devices.

$$E_b = (E_{LUMO} - E_{HOMO}) - E_{ex} \quad (15)$$

Table 10. Exciton binding energy (E_b), first excitation energy (E_{ex}), and energy gap

molecule	E_g (eV)	E_{ex} (eV)	E_b (eV)
TQTP-TPz-TQTP	1.68	1.41	0.27

6. Conclusion

In this study, a first-principles quantum-chemical analysis of the π -conjugated thieno[3,4-b]pyrazine-based system TQTP-TPz-TQTP was performed in order to disclose its electronic structure, optical properties, and thermal stabilities for applications in organic optoelectronic devices. Ground- and excited-state properties were systematically investigated by using Density Functional Theory (DFT) and Time-Dependent (DFT) (TD-DFT) at the B3LYP/6-31G(d,p) level, also employing the range-separated CAM-B3LYP functional to achieve a sound description of charge-transfer excitations.

The geometry optimization indicates that TQTP-TPz-TQTP has a quasi-planar molecular structure, which could lead to efficient π -electron delocalization as well as intramolecular charge transfer (ICT). The frontier molecular orbital energy gap ($E_g = E_{LUMO} - E_{HOMO}$) was calculated to be $E_g = 1.68$ eV, indicative of increased electronic coupling between donor and acceptor moieties. The computed UV-Vis spectra predict intense low-energy transitions in the red and near-infrared region

at $\lambda_{\text{max}} = 877 \text{ nm}$ (TD-B3LYP) / $\lambda_{\text{max}} = 668 \text{ nm}$ (CAM-B3LYP), where the addition of electron-withdrawing substituents enhances ICT and induces a strong bathochromic shift, whereas donor groups stabilize the HOMO level.

Charge transfer properties were also investigated by frontier molecular orbital (FMO), density of states (DOS), and transition density matrix (TDM) analyses, which altogether suggest significant electronic delocalization and desirable excited-state charge separation. Efficient exciton splitting, charge transport, and photovoltaic performances are expected from the calculated E_b of 0.27 eV.

According to the Scharber model, the estimated $V_{\text{oc}} = 0.99 \text{ V}$ and PCE ($\approx 9.6\%$) further indicate the advantageous potential of this compound as a donor material in OPVs from a theoretical simulation perspective. Moreover, the substantially improved static polarizability and first-order hyperpolarizability, as compared to those of urea, testify that the system possesses remarkable nonlinear optical (NLO) response due to the elongated π -conjugation effect and strong donor–acceptor interactions.

In summary, the present computational study shows that rational molecular design of thieno[3,4-b]pyrazine derivatives based on electronic-structure calculations is an efficient way to fine-tune their optoelectronic and NLO properties. Each piece of data demonstrates that the current work provides a solid reference point for asymmetric functionalization, π -conjugation extension and benchmarking with higher-level methodologies as well as against experimental values.

Author contributions

ME also drafted the original version of the manuscript. MC contributed to the interpretation of the results and scientific discussion. MO, and AA performed the theoretical calculations and analyzed the data. TL supervised the project, proposed the initial concept, and coordinated the overall study. MRF and MB wrote the main text of the manuscript. All authors reviewed and approved the final version of the manuscript.

Funding

This research received no financial support.

Declaration of competing interest

The authors declare that they have no known competing financial interests or personal relationships that could have appeared to influence the work reported in this paper.

Acknowledgments

We dedicate this work to the “Moroccan Association of Theoretical Chemists” (MATC) for its pertinent help concerning the programs.

Data availability

Data will be made available on request

The compounds 7b–d and 7f were synthesized according to the procedure previously reported by Cheminet et al. (2020)²². Their structures were confirmed by spectroscopic techniques including ¹H NMR, ¹³C NMR, IR, UV–visible spectroscopy and mass spectrometry. The complete spectral data and characterization details are provided in the Supporting Information section.

References

- [1] Masood M. T. and Shah F. (2012) Dilemma of third world countries: problems facing Pakistan energy crisis as a case in point. *Int. J. Bus. Manag.*, 7(5), 231–243. (<https://doi.org/10.5539/ijbm.v7n5p231>).
- [2] Farghali M., Osman A. I., Mohamed I. M., Chen Z., Chen L., Ihara I., and Rooney D. W. (2023) Strategies to save energy in the context of the energy crisis: a review. *Environ. Chem. Lett.*, 21(4), 2003–2039. (<https://doi.org/10.1007/s10311-023-01591-5>).
- [3] Marszalek M., Nagane S., Ichake A., Humphry-Baker R., Paul V., Zakeeruddin S. M., and Grätzel M. (2013) Structural variations of D– π –A dyes influence on the photovoltaic performance of dye-sensitized solar cells. *RSC Adv.*, 3(21), 7921–7927. (<https://doi.org/10.1039/c3ra22249g>).
- [4] Zhang Y. H. P. (2009) A sweet out-of-the-box solution to the hydrogen economy: Is the sugar-powered car science fiction? *Energy Environ. Sci.*, 2(3), 272–282. (<https://doi.org/10.1039/b818694d>).
- [5] Zahra T., Ahmad K. S., Thomas A. G., Zequine C., Malik M. A., and Gupta R. K. (2020) Organic template-based ZnO embedded MnO₄ nanoparticles: synthesis and evaluation of their electrochemical properties towards clean energy generation. *RSC Adv.*, 10(17), 9854–9867. (<https://doi.org/10.1039/c9ra10472k>).

- [6] Riede M., Spoltore D., and Leo K. (2021) Organic solar cells—The path to commercial success. *Adv. Energy Mater.*, 11(1). (<https://doi.org/10.1002/aenm.202002653>)
- [7] Braga A. F. B., Moreira S. P., Zampieri P. R., Bacchin J. M. G., and Mei P. R. (2008) New processes for the production of solar-grade polycrystalline silicon: a review. *Sol. Energy Mater. Sol. Cells*, 92(4), 418–424. (<https://doi.org/10.1016/j.solmat.2007.10.003>).
- [8] Shafiq Z., Akram N., Zia K. M., Jamil S., Li S., Alhokbany N., and Janjua M. R. S. A. (2025) Unveiling next-generation organic photovoltaics: quantum mechanical insights into non-fullerene donor–acceptor compounds. *Spectrochim. Acta A Mol. Biomol. Spectrosc.*, 330, 125741. (<https://doi.org/10.1016/J.SAA.2025.125741>).
- [9] Duan T., Chen Q., Hu D., Lv J., Yu D., Li G., and Lu S. (2022) Oligothiophene-based photovoltaic materials for organic solar cells: rise, plateau, and revival. *Trends Chem.*, 4(9), 773–791. (<https://doi.org/10.1016/j.trechm.2022.06.007>).
- [10] Cheng P., Li G., Zhan X., and Yang Y. (2018) Next-generation organic photovoltaics based on non-fullerene acceptors: review article. *Nat. Rev. Mater.*, 3, 299–314. (<https://doi.org/10.1038/s41566-018-0104-9>).
- [11] Bouzzine S. M., Abdelaaziz A., Zaid F., Hamidi M., Al-Zahrani F. A. M., and El-Shishtawy R. M. (2024) Investigation of the structural and optoelectronic characteristics in coumarin-based dye-sensitized solar cells, both in isolation and with TiO₂ adsorption. *Comput. Mater. Sci.*, 241, 113043. (<https://doi.org/10.1016/J.COMMATSCI.2024.113043>).
- [12] Adeniyi A. A. and Ajibade P. A. (2017) Computational study of the impact of regeneration and unwanted recombination reactions of Ru(II) phenanthroline compounds used as sensitizers in dye-sensitized solar cells. *Comput. Mater. Sci.*, 139, 301–312. (<https://doi.org/10.1016/J.COMMATSCI.2017.08.011>)
- [13] An K., Zhong W., Peng F., Deng W., Shang Y., Quan H., and Ying L. (2023) Mastering morphology of non-fullerene acceptors towards long-term stable organic solar cells. *Nat. Commun.*, 14(1), 2688. (<https://doi.org/10.1038/s41467-023-38306-x>).
- [14] Peng W., Zhang G., Shao L., Ma C., Zhang B., Chi W., and Zhu W. (2018) Simple-structured small molecule acceptors constructed by a weakly electron-deficient thiazolothiazole core for high-efficiency non-fullerene organic solar cells. *J. Mater. Chem. A*, 6(47), 24267–24276. (<https://doi.org/10.1039/c8ta09370a>).
- [15] Walzer K., Männig B., Pfeiffer M., and Leo K. (2007) Highly efficient organic devices based on electrically doped transport layers. *Chem. Rev.*, 107, 1233–1271. (<https://doi.org/10.1021/cr050156n>).
- [16] Kacimi R., Hayn R., Azaid A., Raftani M., Bejjit L., and Bouachrine M. (2025) Design and computational analysis of benzothiadiazole-fluorene based molecules for organic light-emitting diodes and high-efficiency organic solar cells. *Mater. Sci. Semicond. Process.*, 190, 109356. (<https://doi.org/10.1016/J.MSSP.2025.109356>).
- [17] El Hadjaoui M., Chemek M., Azaid A., Ouabane M., Fouad M. R., Lakhlifi T., and Bouachrine M. (2026) Molecular engineering of thieno[3,4-b]pyrazine-based materials: toward organic photovoltaic applications: DFT and TD-DFT investigations. *Curr. Chem. Lett.* (2026). (<https://doi.org/10.5267/j.ccl.2025.12.005>)
- [18] Azaid A., Abram T., Kacimi R., Sbai A., Lakhlifi T., and Bouachrine M. (2021) Organic materials based with D– π –A structure based on thiophene and anthracene for application in dye-sensitized solar cells. *Mater. Today Proc.*, 45, 7363–7369. (<https://doi.org/10.1016/J.MATPR.2021.01.119>).
- [19] Nebbach D., Agda F., Kaya S., Siddique F., Lakhlifi T., Ajana M. A., and Bouachrine M. (2022) Non-fullerene acceptor IDIC based on indacenodithiophene used as an electron donor for organic solar cells: a computational study. *J. Mol. Liq.*, 348, 118289. (<https://doi.org/10.1016/J.MOLLIQ.2021.118289>).
- [20] Bouzakraoui S., Bouzzine S. M., Bouachrine M., and Hamidi M. (2006) Theoretical investigation of electroluminescent alkoxy substituted 4,4'-bis(2-phenylethenyl)biphenyls as guest in blue OLEDs. *Sol. Energy Mater. Sol. Cells*, 90(10), 1393–1402. (<https://doi.org/10.1016/J.SOLMAT.2005.10.004>).
- [21] Azaid A., Alaqrbeh M., Abram T., Raftani M., Kacimi R., Khaddam Y., and Bouachrine M. (2024) D– π –A push-pull chromophores based on N,N-diethylaniline as a donor for NLO applications: effects of structural modification of π -linkers. *J. Mol. Struct.*, 1295, 136602. (<https://doi.org/10.1016/J.MOLSTRUC.2023.136602>).
- [22] Cheminet N., Nogueira S. L., Benaqqa O., El Malki Z., Bourass M., Cassegrain S., and Serein-Spirau F. (2020) Elaboration of low-band-gap π -conjugated systems based on thieno[3,4-b]pyrazines. *Pure Appl. Chem.*, 92(2), 335–353. (<https://doi.org/10.1515/pac-2018-1009>).
- [23] Cavasotto C. N., Aucar M. G., and Adler N. S. (2019) Computational chemistry in drug lead discovery and design. *Int. J. Quantum Chem.*, 119, e25678. (<https://doi.org/10.1002/qua.25678>).
- [24] Klimeck G., Chen L. Q., Neugebauer J., Kumar S. K., Terasaki I., Kalinin S. V., and Chen L. D. (2015) Design and discovery of materials guided by theory and computation. *NPJ Comput. Mater.*, 1, 15007. (<https://doi.org/10.1038/npjcompumats.2015.7>).
- [25] Agwamba E. C., Louis H., Unimuke T. O., Ameuru U. S., Mathias G. E., Chukwu U. G., and Eno E. A. (2022) Molecular modeling of the photovoltaic properties of amino naphthalene and N-alkylated-isoquinoline dye. *J. Indian Chem. Soc.*, 99(11), 100739. (<https://doi.org/10.1016/J.JICS.2022.100739>).
- [26] Frisch A. (1996) *Gaussian 09W Reference*. Gaussian, Inc.
- [27] Irfan A. and Mahmood A. (2018) Designing of efficient acceptors for organic solar cells: molecular modelling at DFT level. *J. Clust. Sci.*, 29(2), 359–365. (<https://doi.org/10.1007/s10876-018-1338-x>).
- [28] Franco F. C. and Padama A. A. B. (2016) DFT and TD-DFT study on the structural and optoelectronic characteristics of chemically modified donor–acceptor conjugated oligomers for organic polymer solar cells. *Polym. (Guildf.)*, 97, 55–62. (<https://doi.org/10.1016/j.polymer.2016.05.025>).

- [29] Dkhissi A., Ouhib F., Chaalane A., Hiorns R. C., Dagron-Lartigau C., Iratcabal P., and Pouchan C. (2012) Theoretical and experimental study of low band gap polymers for organic solar cells. *Phys. Chem. Chem. Phys.*, 14(16), 5613–5619. (<https://doi.org/10.1039/c2cp40170c>).
- [30] Johansson T., Mammo W., Svensson M., Andersson M. R., and Inganäs O. (2003) Electrochemical bandgaps of substituted polythiophenes. *J. Mater. Chem.*, 13(6), 1316–1323. (<https://doi.org/10.1039/b301403g>).
- [31] Yanai T., Tew D. P., and Handy N. C. (2004) A new hybrid exchange–correlation functional using the Coulomb-attenuating method (CAM-B3LYP). *Chem. Phys. Lett.*, 393(1–3), 51–57. (<https://doi.org/10.1016/J.CPLETT.2004.06.011>)
- [32] Kahn M. L., Sutter J. P., Golhen S., Guionneau P., Ouahab L., Kahn O., and Chasseau D. (2000) Systematic investigation of the nature of the coupling between a Ln(III) ion (Ln = Ce(III) to Dy(III)) and its aminoxyl radical ligands: structural and magnetic characteristics of a series of {Ln(organic radical)₂} compounds and the related {Ln(Nitron)₂} derivatives. *J. Am. Chem. Soc.*, 122(14), 3413–3421. (<https://doi.org/10.1021/ja004655b>).
- [33] Lu T. and Chen F. (2012) Multiwfn: a multifunctional wavefunction analyzer. *J. Comput. Chem.*, 33(5), 580–592. (<https://doi.org/10.1002/jcc.22885>).
- [34] Akram S. J., Iqbal J., Ans M., El-Badry Y. A., Mehmood R. F., and Khera R. A. (2022) Designing of the indacenodithiophene core-based small molecules for optoelectronic applications: a DFT approach. *Sol. Energy*, 237, 108–121. (<https://doi.org/10.1016/J.SOLENER.2022.03.072>).
- [35] Paramasivam M., Gupta A., Raynor A. M., Bhosale S. V., Bhanuprakash K., and Rao V. J. (2014) Small band gap D- π -A- π -D benzothiadiazole derivatives with low-lying HOMO levels as potential donors for applications in organic photovoltaics: a combined experimental and theoretical investigation. *RSC Adv.*, 4(67), 35318–35331. (<https://doi.org/10.1039/C4RA04522F>).
- [36] Ans M., Iqbal J., Eliasson B., Saif M. J., and Ayub K. (2019) Opto-electronic properties of non-fullerene fused-undecacyclic electron acceptors for organic solar cells. *Comput. Mater. Sci.*, 159, 150–159. (<https://doi.org/10.1016/J.COMMATSCI.2018.12.009>).
- [37] Dewar M. J. S. and Thiel W. (1977) Ground states of molecules. 38. The MNDO method: approximations and parameters. *J. Am. Chem. Soc.*, 99, 4899–4907. (<https://doi.org/10.1021/ja00457a004>).
- [38] Lesar A. and Milošev I. (2009) Density functional study of the corrosion inhibition properties of 1,2,4-triazole and its amino derivatives. *Chem. Phys. Lett.*, 483(4–6), 198–203. (<https://doi.org/10.1016/J.CPLETT.2009.10.082>).
- [39] Parr R. G., Szentpály L. V., and Liu S. (1999) Electrophilicity index. *J. Am. Chem. Soc.*, 121(9), 1922–1924. (<https://doi.org/10.1021/ja983494x>).
- [40] Raissi H., Chérif I., Aribi I., Ayachi H., Haj Said A., Ayachi S., and Boubaker T. (2022) Structure–property relationships in para-substituted nitrobenzofurazans: electrochemical, optical, and theoretical analysis. *Chem. Pap.*, 76(7), 4059–4080. (<https://doi.org/10.1007/s11696-022-02150-y>).
- [41] Parr R. G., Donnelly R. A., Levy M., and Palke W. E. (1977) Electronegativity: the density functional viewpoint. *J. Chem. Phys.*, 68(8), 3801–3807. (<https://doi.org/10.1063/1.436185>).
- [42] Mustafa G., Shafiq I., Shaikh Q. U. A., Mustafa A., Zahid R., Rasool F., and Haroon M. (2023) Quantum chemical exploration of A- π 1-D1- π 2-D2-type compounds for the exploration of chemical reactivity, optoelectronic, and third-order nonlinear optical properties. *ACS Omega*, 8(25), 22673–22683. (<https://doi.org/10.1021/acsomega.3c01472>).
- [43] Afolabi S. O., Semire B., Akiode O. K., Afolabi T. A., Adebayo G. A., and Idowu M. A. (2020) Design and theoretical study of phenothiazine-based low bandgap dye derivatives as sensitizers in molecular photovoltaics. *Opt. Quantum Electron.*, 52(11). (<https://doi.org/10.1007/s11082-020-02600-5>).
- [44] Lakshminarayanan S., Jeyasingh V., Murugesan K., Selvapalam N., and Dass G. (2021) Molecular electrostatic potential (MEP) surface analysis of chemo sensors: an extra supporting hand for strength, selectivity & non-traditional interactions. *J. Photochem. Photobiol.*, 6, 100022. (<https://doi.org/10.1016/J.JPAP.2021.100022>).
- [45] Shahab S., Yahyaei H., Sheikhi M., Filippovich L., Zhou H., Kaviani S., and Agabekov V. E. (2021) Two new dichroic dyes: quantum chemical modeling, synthesis, optical properties and their application in polarizing films. *J. Mol. Struct.*, 1239, 130353. (<https://doi.org/10.1016/J.MOLSTRUC.2021.130353>).
- [46] Mohan B., Jana A., Das N., Bharti S., Choudhary M., Muhammad S., and Algarni H. (2019) A dual approach to study the key features of nickel(II) and copper(II) coordination complexes: synthesis, crystal structure, optical and nonlinear properties. *Inorg. Chim. Acta*, 484, 148–159. (<https://doi.org/10.1016/J.ICA.2018.09.037>).
- [47] Bibi S., Shafiq-ur-Rehman, Jia R., Zhang H. X., and Bai F. Q. (2019) Effect of different topological structures (D- π -D and D- π -A- π -D) on the optoelectronic properties of benzo[2,1-B:3,4-B']dithiophene based donor molecules toward organic solar cells. *Sol. Energy*, 186, 311–322. (<https://doi.org/10.1016/J.SOLENER.2019.04.043>).
- [48] Yao H., Cui Y., Qian D., Ponseca C. S. Jr, Honarfar A., Xu Y., and Hou J. (2019) 14.7% efficiency organic photovoltaic cells enabled by active materials with a large electrostatic potential difference. *J. Am. Chem. Soc.*, 141(19), 7743–7750. (<https://doi.org/10.1021/jacs.8b12937>).
- [49] Ostovan A., Mahdavi Z., and Bamdad M. (2017) Evaluation of photovoltaic properties and effective conjugated length of DTTTD-based polymers as donor in BHJ solar cells: quantum chemical approach. *Polym.*, 126, 162–176. (<https://doi.org/10.1016/J.POLYMER.2017.08.044>).
- [50] Hedström S., Henriksson P., Wang E., Andersson M. R., and Persson P. (2014) Light-harvesting capabilities of low band gap donor–acceptor polymers. *Phys. Chem. Chem. Phys.*, 16(45), 24853–24865. (<https://doi.org/10.1039/C4CP03191A>).

- [51] Irfan M., Iqbal J., Sadaf S., Eliasson B., Rana U. A., Ud-din Khan S., and Ayub K. (2017) Design of donor–acceptor–donor (D–A–D) type small molecule donor materials with efficient photovoltaic parameters. *Int. J. Quantum Chem.*, 117(10), e25363. (<https://doi.org/10.1002/qua.25363>).
- [52] Gadisa A., Svensson M., Andersson M. R., and Inganäs O. (2004) Correlation between oxidation potential and open-circuit voltage of composite solar cells based on blends of polythiophenes/fullerene derivative. *Appl. Phys. Lett.*, 84(9), 1609–1611. (<https://doi.org/10.1063/1.1650878>).
- [53] Scharber M. C., Mühlbacher D., Koppe M., Denk P., Waldauf C., Heeger A. J., and Brabec C. J. (2006) Design rules for donors in bulk-heterojunction solar cells: towards 10% energy-conversion efficiency. *Adv. Mater.*, 18(6), 789–794. (<https://doi.org/10.1002/adma.200501717>).
- [54] Adler S. B. (2004) Factors governing oxygen reduction in solid oxide fuel cell cathodes. *Chem. Rev.*, 104(10), 4791–4843. (<https://doi.org/10.1021/cr020724o>).
- [55] Ohkita H., Cook S., Astuti Y., Duffy W., Tierney S., Zhang W., and Durrant J. R. (2008) Charge carrier formation in polythiophene/fullerene blend films studied by transient absorption spectroscopy. *J. Am. Chem. Soc.*, 130(10), 3030–3042. (<https://doi.org/10.1021/ja710273q>).
- [56] Clarke T. M., Ballantyne A. M., Nelson J., Bradley D. D. C., and Durrant J. R. (2008) Free energy control of charge photogeneration in polythiophene/fullerene solar cells: the influence of thermal annealing on P3HT/PCBM blends. *Adv. Funct. Mater.*, 18(24), 4029–4035. (<https://doi.org/10.1002/adfm.200800727>).
- [57] Shoaee S., Clarke T. M., Huang C., Barlow S., Marder S. R., Heeney M., and Durrant J. R. (2010) Acceptor energy level control of charge photogeneration in organic donor/acceptor blends. *J. Am. Chem. Soc.*, 132(37), 12919–12926. (<https://doi.org/10.1021/ja1042726>).
- [58] Thompson B. C. and Fréchet J. M. J. (2008) Polymer-fullerene composite solar cells. *Angew. Chem. Int. Ed.*, 47, 58–77. (<https://doi.org/10.1002/anie.200702506>).
- [59] Duan Y. A., Geng Y., Li H. B., Jin J. L., Wu Y., and Su Z. M. (2013) Theoretical characterization and design of small molecule donor material containing naphthodithiophene central unit for efficient organic solar cells. *J. Comput. Chem.*, 34(19), 1611–1619. (<https://doi.org/10.1002/jcc.23298>).
- [60] Walker B., Liu J., Kim C., Welch G. C., Park J. K., Lin J., and Nguyen T. Q. (2013) Optimization of energy levels by molecular design: evaluation of bis-diketopyrrolopyrrole molecular donor materials for bulk heterojunction solar cells. *Energy Environ. Sci.*, 6(3), 952–962. (<https://doi.org/10.1039/c3ee24351f>).
- [61] Qadir K. W., Mohammadi M. D., Abbas F., and Abdullah H. Y. (2024) Molecular engineering of BTO for superior photovoltaic efficiency: a DFT exploration. *Mater. Chem. Phys.*, 314, 128866. (<https://doi.org/10.1016/J.MATCHEMPHYS.2023.128866>).
- [62] Zhou K., Liu Y., Alotaibi A., Yuan J., Jiang C., Xin J., and Ma W. (2020) Molecular and energetic order dominate the photocurrent generation process in organic solar cells with small energetic offsets. *ACS Energy Lett.*, 5(2), 589–596. (<https://doi.org/10.1021/acscenergylett.9b02697>).
- [63] Kim B. G., Zhen C. G., Jeong E. J., Kieffer J., and Kim J. (2012) Organic dye design tools for efficient photocurrent generation in dye-sensitized solar cells: exciton binding energy and electron acceptors. *Adv. Funct. Mater.*, 22(8), 1606–1612. (<https://doi.org/10.1002/adfm.201101961>).
- [64] El Hadjaoui M., Azaid A., Ouabane M., Chemek M., and Bouachrine M. (2026) Theoretical design and optoelectronic properties of novel donor–acceptor–donor thieno[3,4-b]pyrazine derivatives for organic solar cells. *Curr. Chem. Lett.*, 15(1), 147–160. (<https://doi.org/10.5267/j.ccl.2025.10.003>).
- [65] Muthu S. and Uma Maheswari J. (2012) Quantum mechanical study and spectroscopic (FT-IR, FT-Raman, ¹³C, ¹H, UV) study, first-order hyperpolarizability, NBO analysis, HOMO and LUMO analysis of 4-[(4-aminobenzene)sulfonyl] aniline by ab initio HF and density functional method. *Spectrochim. Acta A Mol. Biomol. Spectrosc.*, 92, 154–163. (<https://doi.org/10.1016/J.SAA.2012.02.056>).
- [66] Govindarasu K. and Kavitha E. (2014) Vibrational spectra, molecular structure, NBO, UV, NMR, first-order hyperpolarizability, analysis of 4-methoxy-4'-nitrobiphenyl by density functional theory. *Spectrochim. Acta A Mol. Biomol. Spectrosc.*, 122, 130–141. (<https://doi.org/10.1016/J.SAA.2013.10.122>).
- [67] Sivaranjani T., Xavier S., and Periandy S. (2015) NMR, FT-IR, FT-Raman, UV spectroscopic, HOMO–LUMO and NBO analysis of cumene by quantum computational methods. *J. Mol. Struct.*, 1083, 39–47. (<https://doi.org/10.1016/J.MOLSTRUC.2014.11.035>).
- [68] Jawaria R., Khan M. U., Ahmed S., Khan M. A., and Ali S. (2019) Synthesis, crystal structure analysis, spectral characterization and nonlinear optical exploration of potent thiosemicarbazones based compounds: a DFT refine experimental study. *Inorg. Chim. Acta*, 486, 162–171. (<https://doi.org/10.1016/J.ICA.2018.10.035>).
- [69] Jawaria R., Khan M. U., Ahmed S., Khan M. A., and Ali S. (2019) Synthesis, crystal structure analysis, spectral characterization and nonlinear optical exploration of potent thiosemicarbazones based compounds: a DFT refine experimental study. *Inorg. Chim. Acta*, 486, 162–171. (<https://doi.org/10.1016/J.ICA.2018.10.035>).
- [70] Li Y. and Ullrich C. A. (2011) Time-dependent transition density matrix. *Chem. Phys.*, 391(1), 157–163. (<https://doi.org/10.1016/J.CHEMPHYS.2011.02.001>).
- [71] Sabir S., Hadia N. M. A., Iqbal J., Mehmood R. F., Akram S. J., Khan M. I., and Khera R. A. (2022) DFT molecular modeling of A2-D-A1-D-A2 type DF-PCIC based small molecule acceptors for organic photovoltaic cells. *Chem. Phys. Lett.*, 806, 140026. (<https://doi.org/10.1016/j.cplett.2022.140026>).
- [72] Yaqoob U., Ayub A. R., Rafiq S., Khalid M., El-Badry Y. A., El-Bahy Z. M., and Iqbal J. (2021) Structural, optical and photovoltaic properties of unfused non-fullerene acceptors for efficient solution-processable organic solar cells

(estimated PCE greater than 12.4%): a DFT approach. *J. Mol. Liq.*, 341, 117428. (<https://doi.org/10.1016/j.molliq.2021.117428>).

- [73] Mehboob M. Y., Hussain R., Irshad Z., and Adnan M. (2021) Enhancement in the photovoltaic properties of hole transport materials by end-capped donor modifications for solar cell applications. *Bull. Korean Chem. Soc.*, 42(4), 597–610. (<https://doi.org/10.1002/bkcs.12238>).



© 2026 by the authors; licensee Growing Science, Canada. This is an open access article distributed under the terms and conditions of the Creative Commons Attribution (CC-BY) license (<http://creativecommons.org/licenses/by/4.0/>).